Evanescent field of vectorial highly non-paraxial beams

R. Martínez-Herrero[1], P. M. Mejías[1*], and A. Carnicer[2]

[1] Departamento de Óptica, Facultad de Ciencias Físicas,Universidad Complutense de Madrid, 28040-Madrid, Spain
[2] Departamento de Física Aplicada y Óptica Facultad de Física, Universidad de Barcelona, 08028-Barcelona, Spain
Corresponding author: pmmejias@fis.ucm.es

Abstract: In terms of the Fourier spectrum, a simple but general analytical expression is given for the evanescent field associated to a certain kind of non-paraxial exact solutions of the Maxwell equations. This expression enables one to compare the relative weight of the evanescent wave with regard to the propagating field. In addition, in those cases in which the evanescent term is significant, the magnitude of the field components across the transverse profile (including the evanescent features) can be determined. These results are applied to some illustrative examples.

OCIS codes: Electromagnetic Optics (260.2110); Polarization (260.5430); Physical Optics (260.0260)

References and Links

1. G. P. Agrawal and M. Lax, "Free-space wave propagation beyond the paraxial approximation," Phys. Rev. A **27**, 1693-1695 (1983).
2. D. G. Hall, "Vector-beam solutions of Maxwell's wave equations," Opt. Lett. **21**, 9-11 (1996).
3. P. Varga and P. Török, "Exact and approximate solutions of Maxwell's equations for a confocal cavity," Opt. Lett. **21**, 1523-1525 (1996).
4. A. Doicu and T. Wriedt, "Plane wave spectrum of electromagnetic beams," Opt. Commun. **136**, 114-124 (1997)
5. S. R. Seshadri, "Electromagnetic Gaussian beam," J. Opt. Soc. Am. A **15**, 2712-2719 (1998).
6. P. Varga. P. Török, "The Gaussian wave solution of Maxvell's equations and the validity of the scalar wave approximation," Opt. Commun. **152**, 108-118 (1998).
7. S. R. Seshadri, "Partially coherent Gaussian Schell-model electromagnetic beam," J. Opt. Soc. Am. A **16**, 1373-1380 (1999).
8. T. Setala, A. T. Friberg and M. Kaivola, "Decomposition of the point-dipole field into homogeneous and evanescent parts," Phys. Rev. E **59**, 1200-1206 (1999).
9. A. V. Shchegrov and P. S. Carney, "Far-field contribution to the electromagnetic Green's tensor from evanescent modes," J. Opt. Soc. Am. A, **16**, 2583-2584 (1999).
10. C. J. R. Sheppard, S. Saghafi, "Electromagnetic Gaussian beams beyond the paraxial approximation," J. Opt. Soc. Am. A **16**, 1381-1386 (1999).
11. S. R. Seshadri, "Average characteristics of partially coherent electromagnetic beams," J. Opt. Soc. Am. A **17**, 780-789 (2000).
12. C. J. R. Sheppard, "Polarization of almost-planes waves," J. Opt. Soc. Am. A **17**, 335-341 (2000).
13. R. Martínez-Herrero, P. M. Mejías, S. Bosch, A. Carnicer, "Vectorial structure of nonparaxial electromagnetic beams," J. Opt. Soc. Am. A **18**, 1678-1680 (2001).
14. J. Tervo and J. Turunen, "Self-imaging of electromagnetic fields," Opt. Express **9**, 622-630 (2001).
15. P. Pääkkönen, J. Tervo, P. Vahimaa, J. Turunen and F. Gori, General vectorial decomposition of electromagnetic fields with application to propagation-invariant and rotating fields," Opt. Express **10**, 949-959 (2002).
16. C. G. Chen, P. T. Konkola, J. Ferrera, R. K. Heilman and M. L. Schattenburg, "Analyses of vector Gaussian beam propagation and the validity of paraxial and spherical approximation," J. Opt. Soc. Am. A **19**, 404-412 (2002).
17. R. Borghi, A. Ciattoni and M. Santarsiero, "Exact axial electromagnetic field for vectorial Gaussian and flattened Gaussian boundary distributions," J. Opt. Soc. Am. A **19**, 1207-1211 (2002).
18. A Ciattoni, B. Crosignani and P. Di Porto, "Vectorial analytical description of propagation of a highly nonparaxial beam," Opt. Commun. **202**, 17-20 (2002).

#90265 - $15.00 USD Received 29 Nov 2007; revised 10 Jan 2008; accepted 24 Jan 2008; published 15 Feb 2008

19. P. M. Mejías, R. Martínez-Herrero, G. Piquero and J. Movilla, "Parametric characterization of the spatial structure of non-uniformly polarized laser beams," Progr. Quantum Electron. **26**, 65-130 (2002).
20. H. F. Arnoldus and J. T. Foley, "Traveling and evanescent fields of an electric point dipole," J. Opt. Soc. Am. A **19**, 1701-1711 (2002).
21. N. I. Petrov, "Evanescent and propagating fields of a strongly focused beam, " J. Opt. Soc. Am. A **20**, 2385-2389 (2003).
22. K. Duan and B. Lü, "Polarization properties of vectorial nonparaxial Gaussian beam in the far field," Opt. Lett. **30**, 308-310 (2005).
23. G. Zhou, X. Chu and L. Zhao, "Propagation characteristics of TM Gaussian beam," Opt. Laser Technol. **37**, 470-474 (2005).
24. K. Belkebir, P. C. Chaumet and A. Sentetac, "Influence of multiple scatering on three-dimensional imaging with optical diffraction tomography," J. Opt. Soc. Am. A **23**, 586-595 (2006).
25. R. Martínez-Herrero, P. M. Mejías, S. Bosch and A. Carnicer, "Structure of the transverse profile of Gaussian-model non-paraxial electromagnetic beams," J. Opt. A: Pure Appl. Opt. **8**, 524-530 (2006).
26. P. C. Chaumet, "Fully vectorial highly nonparaxial beam close to the waist," J. Opt. Soc. Am. A **23**, 3197-3202 (2006).
27. H. Guo, J. Chen and S. Zhuang, "Vector plane spectrum of an arbitrary polarized electromagnetic wave," Opt. Express **14**, 2095-2100 (2006).
28. G. C. Sherman, J. J. Stamnes and E. Lalor, "Asymptotic approximations to angular-spectrum representations," J. Math. Phys. **17**, 760-776 (1976).

1. Introduction

The propagation of the non-paraxial electromagnetic beams has been extensively investigated in the last decade.[1-27] In fact, non-paraxial fields have revealed to be very useful in Optics, as occurs, for example, in high-resolution microscopy, particle trapping, high-density recording and tomography.[24] At the waist plane, the transverse size of such strongly-focused beams is smaller than the wavelength. Usually, the field amplitude is evaluated far enough from the waist in order to neglect the contribution of the evanescent waves. However, this kind of waves can be of considerable interest because of the possibility of subwavelength resolution, beyond the diffraction limit.

In the present paper, attention is focused on two main subjects, namely, to get exact solutions (without approximation) of the Maxwell equations behaving as highly non-paraxial beams, and to investigate the analytical structure and the field magnitude and polarization features of the associated evanescent-field distributions.

In the literature, different vectorial formulations of non-paraxial beams have been explored (for example, in terms of the Hertz vectors, [3,6,12] or by using the complex-source-point mode[10]). Among them, several kind of representations of an electromagnetic beam based on its angular plane-wave spectrum have been reported in recent years.[13,19,23,25,26,27] Such kind of decomposition is particularly useful because it enables to separate the contribution of the propagating and evanescent waves [8,9,20,21,26] (also called homogeneous and inhomogeneous parts of the spectrum [28]). When the contribution of the evanescent waves is negligible, it has been shown [13,19,25] that the electric field solution can be written as the sum of two terms: one of them is transverse to the propagation direction; another one exhibits a non-zero longitudinal component and its associated magnetic field is also transverse. This analytical structure differs from alternative proposals also based on the angular spectrum (see, for example, Ref. 26). In the present work we will extend this TE- and TM-decomposition to include the evanescent part of the plane-wave representation.

Accordingly, the paper is arranged as follows. In the next section, the formalism and the key definitions to be used in the rest of the paper are introduced. In Section 3 the electric field solution proposed in Section 2 is decomposed into its propagating and evanescent parts. It will be derived a general expression with separate contributions of TE, TM and evanescent terms. In particular it will be shown the appearance of pure TE-solutions for the global field (including the evanescent wave). Both, the field magnitude and the polarization structure of the evanescent field are computed in Section 4 for several illustrative cases in which this kind of waves are significant. The concept of closest field is considered, and the analytical

#90265 - $15.00 USD Received 29 Nov 2007; revised 10 Jan 2008; accepted 24 Jan 2008; published 15 Feb 2008

difference between our procedure and other recently proposed solutions [26] is discussed in the same section. Finally, the main conclusions are summarized in Section 5.

2. Formalism and key definitions

The propagation of a time-harmonic electromagnetic field in homogeneous isotropic media is described by means of the Maxwell equations

$$\nabla \times \boldsymbol{H} + ik\boldsymbol{E} = 0, \tag{1.a}$$

$$\nabla \times \boldsymbol{E} - ik\boldsymbol{H} = 0, \tag{1.b}$$

$$\nabla \cdot \boldsymbol{E} = \nabla \cdot \boldsymbol{H} = 0, \tag{1.c}$$

where $\boldsymbol{E}$ and $\boldsymbol{H}$ represent the spatial structure of the electric and magnetic fields, respectively, $k = n\omega/c$ is the wavenumber, n the refractive index of the medium, ω the angular frequency of the radiation and c the speed of light in vacuum. As is well known, the fields $\boldsymbol{E}$ and $\boldsymbol{H}$ can be expressed in terms of their angular plane-wave spectrum,

$$\boldsymbol{E}(x,y,z) = \int \tilde{\boldsymbol{E}}(u,v,z)\exp\left[\mathrm{i}k(xu+yv)\right]dudv, \tag{2}$$

and a similar expression for $\boldsymbol{H}$. In Eq. (2) $\tilde{\boldsymbol{E}}$ denotes the spatial Fourier transform of $\boldsymbol{E}$ (the same would apply for $\tilde{\boldsymbol{H}}$). Although x, y and z should be considered, in principle, as equivalent directions, for simplicity we will choose z as the direction of propagation of the beam. Moreover, in the present paper we will be concerned with the values of the field at planes transverse to this axis.

In terms of the angular spectrum, the Maxwell equations become

$$\boldsymbol{L} \times \tilde{\boldsymbol{H}} + ik\tilde{\boldsymbol{E}} = 0 \tag{3.a}$$

$$\boldsymbol{L} \times \tilde{\boldsymbol{E}} - ik\tilde{\boldsymbol{H}} = 0, \tag{3.b}$$

$$\boldsymbol{L} \cdot \tilde{\boldsymbol{E}} = \boldsymbol{L} \cdot \tilde{\boldsymbol{H}} = 0, \tag{3.c}$$

where $\boldsymbol{L} \equiv (\mathrm{i}ku, \mathrm{i}kv, \partial/\partial z)$. Instead of using Cartesian coordinates, for the sake of convenience we will next handle cylindrical coordinates R, θ and z, along with polar coordinates, ρ and ϕ for the transverse Fourier-transform variables u, v. Thus we have

$$x = R\cos\theta \quad y = R\sin\theta \tag{4.a}$$

$$u = \rho\cos\phi \quad v = \rho\sin\phi. \tag{4.b}$$

Taking this into account, a general solution of Eqs. (3) can formally be written as follows

$$\tilde{\boldsymbol{E}}(\rho,\phi,z) = \tilde{\boldsymbol{E}}_{\boldsymbol{0}}(\rho,\phi)\exp(ikz\xi), \tag{5}$$

with the relations

$$\tilde{\boldsymbol{E}}_{\boldsymbol{0x}}\sigma_x + \tilde{\boldsymbol{E}}_{\boldsymbol{0y}}\sigma_y + \tilde{\boldsymbol{E}}_{\boldsymbol{0z}}\sigma_z = 0, \tag{6}$$

and

$$\tilde{\boldsymbol{H}}(\rho,\phi,z) = (\sigma \times \tilde{\boldsymbol{E}}_{\boldsymbol{0}})\exp(ikz\xi), \tag{7}$$

where

#90265 - $15.00 USD Received 29 Nov 2007; revised 10 Jan 2008; accepted 24 Jan 2008; published 15 Feb 2008

$$\xi = \sqrt{1-\rho^2} \quad \rho \le 1, \tag{8.a}$$

$$\xi = i\sqrt{\rho^2 - 1} \quad \rho > 1, \tag{8.b}$$

and $\boldsymbol{\sigma} = (\sigma_x, \sigma_y, \sigma_z) = (\rho\cos\phi, \rho\sin\phi, \xi)$. It is clear from Eq. (8.b) that the third component of $\boldsymbol{\sigma}$ would be, in general, a complex number whose physical meaning will be apparent later. Note also that condition (6) is a direct consequence of the Maxwell equation $\nabla \cdot \boldsymbol{E} = 0$.

Now, based on the plane-wave spectrum given by Eq. (5), we finally express the electric field solution of the Maxwell equations in the form

$$\boldsymbol{E}(R,\theta,z) = \int_0^{\infty}\int_0^{2\pi} \tilde{\boldsymbol{E}}_0(\rho,\phi)\exp\left[ik\rho R\cos(\theta-\phi)\right]\exp(ikz\xi)\rho d\rho d\phi, \tag{9}$$

where $\tilde{\boldsymbol{E}}_0$ should fulfill condition (6).

3. Field decomposition into propagating and evanescent waves

To go further into the analysis of this general solution, let us write the field $\boldsymbol{E}(R,\theta,z)$, given by Eq. (9), as the sum of two terms

$$\boldsymbol{E}(R,\theta,z) = \boldsymbol{E}_{pr}(R,\theta,z) + \boldsymbol{E}_{ev}(R,\theta,z), \tag{10}$$

where

$$\boldsymbol{E}_{pr}(R,\theta,z) = \int_0^{1}\int_0^{2\pi} \tilde{\boldsymbol{E}}_0(\rho,\phi)\exp\left[ik\rho R\cos(\theta-\phi)\right]\exp(ikz\xi)\rho d\rho d\phi, \tag{11.a}$$

$$\boldsymbol{E}_{ev}(R,\theta,z) = \int_1^{\infty}\int_0^{2\pi} \tilde{\boldsymbol{E}}_0(\rho,\phi)\exp\left[ik\rho R\cos(\theta-\phi)\right]\exp(ikz\xi)\rho d\rho d\phi. \tag{11.b}$$

It is well known that the term $\boldsymbol{E}_{\rm pr}$ should be understood as a superposition of plane waves propagating in the directions specified by ρ and ϕ. Some authors [28] refer to this term as the homogeneous part of the angular spectrum. The field $\boldsymbol{E}_{\rm pr}$ would then represent the contribution of the propagating (homogeneous) waves. The second term, $\boldsymbol{E}_{\rm ev}$, should be considered as a superposition of inhomogeneous waves that decay at different rates in the z-direction. In other words, this term accounts for the contribution of the evanescent field. As we pointed out in the Introduction, our present interest is focused on those cases in which the evanescent part of the exact solution is significant enough (as we will see in the examples shown in Section 4, this would occur in the highly non-paraxial case at the neighbourhood of the initial plane z = 0).

To handle this problem we will next extend the formalism used in previous papers,[13,19,25] and write the field $\boldsymbol{E}(R,\theta,z)$, given by Eq. (10), in the alternative equivalent form

#90265 - $15.00 USD Received 29 Nov 2007; revised 10 Jan 2008; accepted 24 Jan 2008; published 15 Feb 2008

$$\boldsymbol{E}(R,\theta,z)=\int_0^1\int_0^{2\pi} a(\rho,\phi)\boldsymbol{e_1}(\phi)\exp\left[\mathrm{i}k\boldsymbol{s}\cdot\boldsymbol{r}\right)\rho d\rho d\phi$$
$$+\int_0^1\int_0^{2\pi} b(\rho,\phi)\boldsymbol{e_2}(\rho,\phi)\exp\left[\mathrm{i}k\boldsymbol{s}\cdot\boldsymbol{r}\right)\rho d\rho d\phi \qquad (12)$$
$$+\int_1^{\infty}\int_0^{2\pi} \left[a(\rho,\phi)\boldsymbol{e_1}(\phi)+b_{ev}(\rho,\phi)\boldsymbol{e_{ev}}(\rho,\phi)\right]\exp\left[\mathrm{i}k\boldsymbol{s_{ev}}\cdot\boldsymbol{r}\right)\rho d\rho d\phi$$

where

$$\boldsymbol{e}_1=(\sin\phi,-\cos\phi,0)\,, \qquad (13.a)$$

$$\boldsymbol{e}_2=(\sqrt{1-\rho^2}\cos\phi,\sqrt{1-\rho^2}\sin\phi,-\rho) \qquad (13.b)$$

and

$$\boldsymbol{s}(\rho,\phi)=\left(\rho\cos\phi,\rho\sin\phi,\sqrt{1-\rho^2}\right),\ \text{with}\ \rho\in[0,1] \qquad (13.c)$$

denote a triad of mutually orthogonal unitary vectors, and

$$\boldsymbol{e_{ev}}=\frac{1}{\sqrt{2\rho^2-1}}(i(\rho^2-1)^{1/2}\cos\phi,i(\rho^2-1)^{1/2}\sin\phi,-\rho) \qquad (14.a)$$

$$\boldsymbol{s_{ev}}=(\rho\cos\phi,\rho\sin\phi,i(\rho^2-1)^{1/2})\,,\ \text{with}\ \rho\in[1,\infty], \qquad (14.b)$$

are formally vectors with complex components. In Eq. (12), $\boldsymbol{s}$ indicates the propagation direction of each plane wave associated to $\tilde{\boldsymbol{E}}_0$. Note that the vectors $\boldsymbol{s}$ and $\tilde{\boldsymbol{E}}_0$ are connected through the Maxwell´s divergence equation (condition (6)) in the interval $\rho\in[0,1]$. The vectors $\boldsymbol{e}_1$ and $\boldsymbol{e}_2$ can be considered as reference axes with respect to which the components of $\tilde{\boldsymbol{E}}_0$ can be given.

Concerning the evanescent term, the structure of $\boldsymbol{s}_{\mathrm{ev}}$ (see Eq. (14.b) assures the fulfilment of condition (6) when $\rho\in[1,\infty]$. In addition, for this range of values of ρ, vectors $\boldsymbol{e}_1$ and $\boldsymbol{e}_{\mathrm{ev}}$ constitute now the two-dimensional reference basis. It should be noted that the choice of the above reference vectors, namely, $\boldsymbol{e}_1$, $\boldsymbol{e}_2$ and $\boldsymbol{e}_{\mathrm{ev}}$, characterizes the formalism handled in the present paper. A final remark should be added with regard to the notation used to define the inner product: In the present paper, $\boldsymbol{a}\cdot\boldsymbol{b}$ should be understood as $a_x b_x^* + a_y b_y^* + a_z b_z^*$, where * means conjugation.

Going back to Eq. (12), we see that the functions $a(\rho, \phi)$, $b(\rho, \phi)$ and $b_{\mathrm{ev}}(\rho, \phi)$ contain the complete information about the Fourier-transform spectrum of the global field (cf. Eq. (5)): In fact, these functions can be inferred from $\tilde{\boldsymbol{E}}_0$ as follows

$$a(\rho,\phi)=\tilde{\boldsymbol{E}}_0\cdot\boldsymbol{e_1}\,, \qquad (15.a)$$

$$b(\rho,\phi)=\tilde{\boldsymbol{E}}_0\cdot\boldsymbol{e_2}\,, \qquad (15.b)$$

#90265 - $15.00 USD Received 29 Nov 2007; revised 10 Jan 2008; accepted 24 Jan 2008; published 15 Feb 2008

$$b_{ev}(\rho,\phi) = \tilde{\boldsymbol{E}}_{\boldsymbol{0}} \cdot \boldsymbol{e}_{\boldsymbol{ev}} \tag{15.c}$$

As is known in the literature,[13,19,25] the first term that appears in the right-hand side of Eq. (12) represents a superposition of plane waves that generate a pure transverse field, $\boldsymbol{E}_{\mathrm{TE}}$, without longitudinal component (E_z=0). The second term, $\boldsymbol{E}_{\mathrm{TM}}$, gives [13] an electric field (perpendicular to $\boldsymbol{E}_{\mathrm{TE}}$ at the far field) whose associated magnetic field, $\boldsymbol{H}_{\mathrm{TM}}$, is also orthogonal to the propagation axis *z*. This structure of the propagating field essentially follows our particular choice of the orthogonal reference axes, $\boldsymbol{e}_1$, $\boldsymbol{e}_2$ and $\boldsymbol{s}$. In the present work the novelty arises from the third term, which contains the evanescent part, understood as a superposition of inhomogeneous waves whose constant phase surfaces are planes orthogonal to the transverse (non-unitary) vector $\boldsymbol{s}_0$, namely,

$$\boldsymbol{s}_{\boldsymbol{0}} = (\rho\cos\phi, \rho\sin\phi, 0), \tag{16}$$

and whose constant-amplitude planes are perpendicular to the z-axis. We thus see that the formal structure of the evanescent part of our solution is similar to that of the propagating field, a result not previously reported for this type of waves to our knowledge. Furthermore, it follows at once from Eqs. (15) that the global solution (12) (propagating + evanescent terms) behaves as a pure transverse field if and only if functions $b(\rho, \phi)$ and $b_{\mathrm{ev}}(\rho, \phi)$ vanish.

Before applying the above expressions to particular cases, it is interesting to remark several advantages of Eq. (12): It provides a general exact solution of the Maxwell equations, which is valid for both, paraxial and strongly-focused beams. Any particular field is then defined by its angular spectrum $\tilde{\boldsymbol{E}}_{\boldsymbol{0}}$ at some initial plane. Furthermore, as we will see in the next section, the field magnitude and polarization features of the transverse profile of any vectorial beam can be computed in a direct way from Eq. (12). In particular, the third term of this equation provides a simple but general procedure to obtain the evanescent field associated to the exact solution given by Eq. (9). In addition, the separate contribution of TE-, TM- and evanescent parts of the electric field allows one to compare the weight of these terms (for example, by comparing the respective square modulus, integrated throughout the beam profile). Consequently, one can determine the ranges of the propagation distance and of the beam size for which the evanescent waves are not negligible. It should also be noted that the evanescent term involves the sum $(\tilde{\boldsymbol{E}}_{\boldsymbol{0}} \cdot \boldsymbol{e}_{\boldsymbol{1}})\boldsymbol{e}_{\boldsymbol{1}} + (\tilde{\boldsymbol{E}}_{\boldsymbol{0}} \cdot \boldsymbol{e}_{\boldsymbol{ev}})\boldsymbol{e}_{\boldsymbol{ev}}$, which can be understood as the projection vector $\tilde{\boldsymbol{E}}_{\boldsymbol{0}}$ onto the subspace generated by $\boldsymbol{e}_1$ and $\boldsymbol{e}_{\mathrm{ev}}$. A similar interpretation led to the concept of "closest" field to a given vector-field solution, introduced not long ago [13] for the propagating term $\boldsymbol{E}_{\mathrm{pr}}$ of the general solution.

In the next section we will use Eqs. (12), (14) and (15) to describe the evanescent structure of the vectorial field closest (in the above algebraic sense) to a polarized Gaussian beam.

4. Numerical examples

It is well known that the widely used pure-transverse linearly-polarized Gaussian field does not satisfy the condition $\nabla\cdot\boldsymbol{E}$ = 0, so it cannot represent an exact solution of the Maxwell equations. In such a model, the vector plane-wave spectrum is represented by the function

$$\tilde{\boldsymbol{f}}(\rho,\phi) = C\exp(-\frac{\rho^2}{D^2})(1,0,0), \tag{17}$$

where *C* is a normalization constant, $D = 1/k\omega_0$ is a constant proportional to the beam divergence at the far field, and ω_0 is the 1/e intensity beam radius of the Gaussian factor at the near field. To derive an exact non-paraxial solution based on the paraxial Gaussian model, one can follow alternative procedures. On the one hand (see, for example, Ref. 26), we may consider that the x- and y-components of the field at the initial transverse plane *z* = 0 have a Gaussian structure. The angular spectrum of each transverse component would then be obtained by using the inverse Fourier transform. In addition, the plane-wave spectrum

#90265 - $15.00 USD Received 29 Nov 2007; revised 10 Jan 2008; accepted 24 Jan 2008; published 15 Feb 2008

associated to the longitudinal component E_z is analytically inferred from Eq. (6). The electric field vector $\boldsymbol{E}(\boldsymbol{r}) = (E_x, E_y, E_z)$ (including its evanescent part) would finally evolve in the $z > 0$ half-space according with well-known integral expressions.[26] The transverse components of this solution would therefore exhibit a Gaussian profile across the plane z = 0.

In the present work an alternative treatment is used: We start from the Gaussian spectrum given by Eq. (17) and calculate the inner products $\tilde{\boldsymbol{f}} \cdot \boldsymbol{e}_1 = a(\rho,\phi)$; $\tilde{\boldsymbol{f}} \cdot \boldsymbol{e}_2 = b(\rho,\phi)$; and $\tilde{\boldsymbol{f}} \cdot \boldsymbol{e}_{ev} = b_{ev}(\rho,\phi)$. We get

$$a(\rho,\phi) = C \sin\phi \exp(-\rho^2 / D^2), \tag{18.a}$$

$$b(\rho,\phi) = C \cos\phi \sqrt{1-\rho^2} \exp(-\rho^2 / D^2), \tag{18.b}$$

$$b_{ev}(\rho,\phi) = -\frac{i}{\sqrt{2\rho^2 - 1}} C \cos\phi (\rho^2 - 1)^{1/2} \exp(-\rho^2 / D^2). \tag{18.c}$$

An exact field solution is then obtained after substitution of functions *a*, *b* and b_{ev} into Eq. (12). This solution should be considered as the generalization (which now includes the evanescent part) of the so-called "closest" field associated to the (paraxial) Gaussian model. Note that our solution should be considered as the field closest (in an algebraic sense) to the Gaussian model (in this connection, recall that functions *a*, *b* and b_{ev} give the projections of $\tilde{\boldsymbol{f}}$ onto $\boldsymbol{e}_1$, $\boldsymbol{e}_2$ and $\boldsymbol{e}_{ev}$, respectively). Note also that, although the above discussion has considered the Gaussian case, it can immediately be extended to a general function $\tilde{\boldsymbol{f}}(\rho,\phi)$.

In the example we are studying, the terms $\boldsymbol{E}_{TE}$ and $\boldsymbol{E}_{TM}$, associated to the propagating waves, were studied elsewhere:[13,19,25]. It was shown that the transverse part (E_x, E_y) of the propagating field closely resembles both, the profile irradiance and the polarization distribution of a conventional (paraxial) Gaussian beam (of course, the presence of a longitudinal z-component involves a conceptually important difference with regard to the paraxial model). It should be pointed out that, for the beam size and the propagation distances considered in those papers, the influence of the evanescent waves was negligible. In the present paper, however, we are basically interested on the evanescent field (cf. Eq. 11.b)). Accordingly, we have to choose parametric values for which the evanescent behaviour becomes significant.

Figure 1 can help to clarify this point. In the figure we plot the ratio $\Delta = |I_{pr} - I_{ev}| / I_{pr}$ for $\omega_0 = 0.1\lambda$ (highly non-paraxial case) at different distances *z* from the initial plane *z* = 0, where

$$I_{pr} = \int_0^1 \int_0^{2\pi} \left[|a(\rho,\phi)|^2 + |b(\rho,\phi)|^2 \right] \rho d\rho d\phi, \tag{19.a}$$

$$I_{ev} = \int_1^{\infty} \int_0^{2\pi} \left[|a(\rho,\phi)|^2 + |b_{ev}(\rho,\phi)|^2 \right] \exp(-2kz\sqrt{\rho^2 - 1}) \rho d\rho d\phi. \tag{19.b}$$

#90265 - $15.00 USD Received 29 Nov 2007; revised 10 Jan 2008; accepted 24 Jan 2008; published 15 Feb 2008

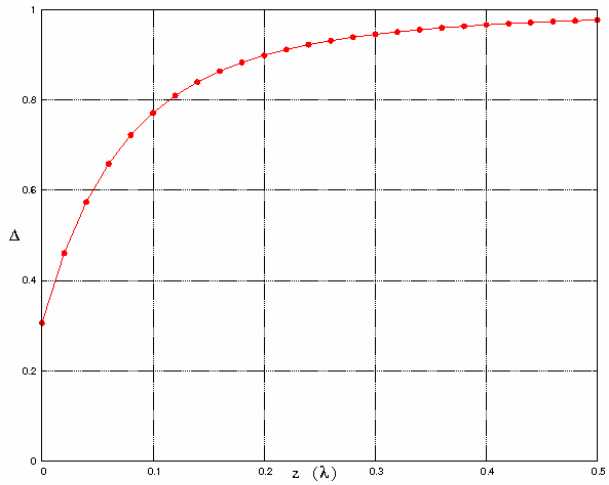

Fig. 1. Ratio Δ in terms of the propagation distance z for the field defined by Eqs. (18), with $\omega_0 = 0.1\lambda$ (highly non-paraxial case).

In other words, I_{pr} and I_{ev} compute the (integrated) squared modulus of the propagating and evanescent fields, respectively. Thus the ratio Δ provides direct information about the importance of the propagating-field solution: Δ ranges from zero (the field is purely evanescent) to 1 (the evanescent term vanishes). For the field we are considering, the evanescent waves are significant enough for propagation distances not longer than, say, λ. Of course, if the waist size ω_0 increases, the relative weight of $\boldsymbol{E}_{ev}$ would drastically reduce, as it should be expected. For example, when $\omega_0 \approx 0.2\lambda$, the distance for noticeable evanescent waves does not exceed 0.1λ.

Once we have determined the appropriated ranges for ω_0 and z, we will show the evanescent structure involved in the closest-field solution associated to a Gaussian beam.

Figures 2, 3 and 4 describe the transverse distributions of the squared modulus of the electric field components of i) propagating waves (Fig. 2); ii) evanescent waves (Fig. 3); and iii) global field (Fig. 4). In these figures we have chosen the values $\omega_0 = 0.1\lambda$ and $z = 0.1\lambda$ (recall that the angular spectrum is defined by Eqs. (18)). In all the figures, abcises and ordinates correspond to the conventional transverse Cartesian axes x and y, respectively. The length of the side of each square frame is 8 λ. Within such frames, the red colour has been associated to the peak value. Furthermore, integration over the entire transverse plane has been normalised to 1 in Fig. 4(d). The rest of the plots are then referred to this value. For example, in Fig. 3(d) the integration gives the value 0.19. This means that the global evanescent field contributes to the overall combined field (propagating + evanescent waves) in a percentage of 19 % (and analogously for the other figures).

In addition, Fig. 2(a) shows that $(|E_x|^2)_{pr}$ is significant on a region whose transverse size along x is nearly λ. This value reduces to 0.5λ for $(|E_x|^2)_{ev}$ in Fig. 3(a). Accordingly, it should be expected that the size of the region over which is significant enough the squared modulus of the x-component of the combined field would closely take the intermediate value $\approx 0.7\lambda$, in agreement with Fig. 4(a). A similar interpretation applies for the rest of the figures.

Finally, from the comparison of Figs. 2 and 3, we see the qualitative agreement (a scale factor apart) between the transverse spatial distribution of the propagating and evanescent fields.

It should be noted that no approximation has been used to compute the electric-field solution shown in the above figures. This is particularly remarkable in the case of the evanescent field, usually neglected in the literature.

#90265 - $15.00 USD Received 29 Nov 2007; revised 10 Jan 2008; accepted 24 Jan 2008; published 15 Feb 2008

For comparative purposes, let us also determine the closest field associated to a typical circularly-polarized Gaussian beam. In such a case, instead of using Eq. (17), the vector function $\tilde{\boldsymbol{f}}(\rho,\phi)$ now reads

$$\tilde{\boldsymbol{f}}(\rho,\phi) = C\exp(-\frac{\rho^2}{D^2})(1,i,0)\,, \tag{20}$$

where ω_0 and z take the same values as before. The characteristics of the associated closest-field solution are reported in Figs. 5, 6 and 7. As expected, all the graphics (c) and (d) show rotational symmetry. Note also the different spatial structure exhibited by the evanescent wave with regard to the former case (see Figs. 3 and 6). It should also be mentioned the similar contributions (percentages) involved in the linear and circular cases, associated to the z-components (figures (c)) and to the global waves (figures (d)).

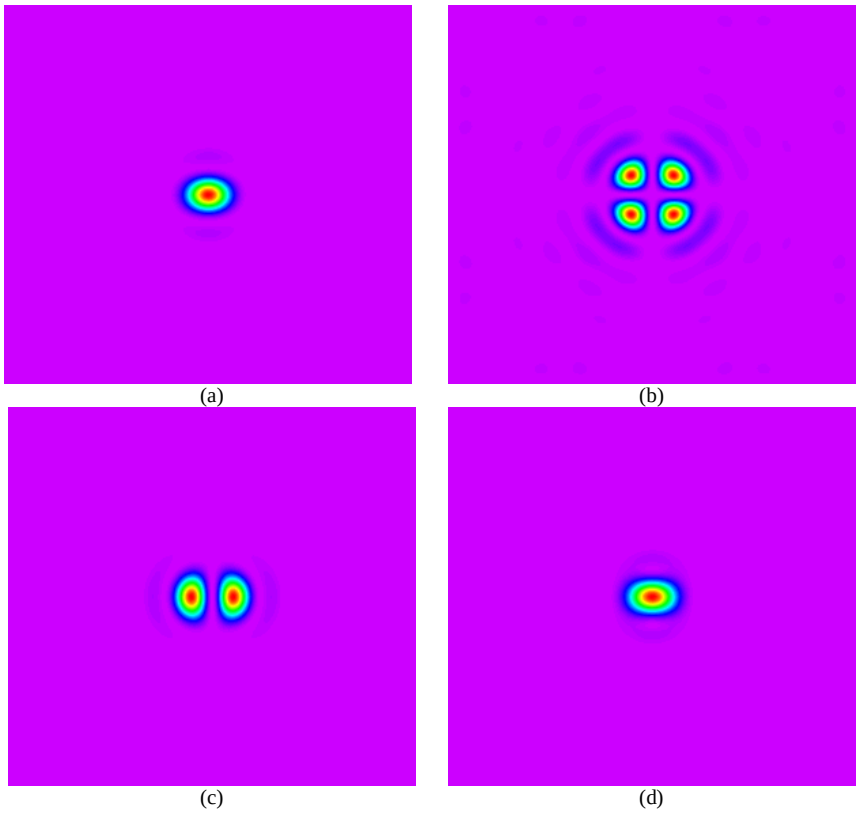

Fig. 2. Transverse distributions (pseudocolour) of the squared modulus of the propagating waves for the field given by Eqs. (18). In this figure, $\omega_0 = 0.1\lambda$ and the field magnitude is computed after propagating a distance $z = 0.1\lambda$. Abcises and ordinates follow the conventional Cartesian representation, namely, abcises are parallel to the lines of writing and ordinates are orthogonal. (a) plot of $(|E_x|^2)_{pr}$; (b) $(|E_y|^2)_{pr}$; (c) $(|E_z|^2)_{pr}$; (d) $(|E_x|^2 + |E_y|^2 + |E_z|^2)_{pr}$. Integration throughout the transverse plane gives the values (a) 0.69; (b) 0.035; (c) 0.085; (d) 0.81. These values have been normalised with respect to that of Fig. 4.d (see below).

#90265 - $15.00 USD Received 29 Nov 2007; revised 10 Jan 2008; accepted 24 Jan 2008; published 15 Feb 2008

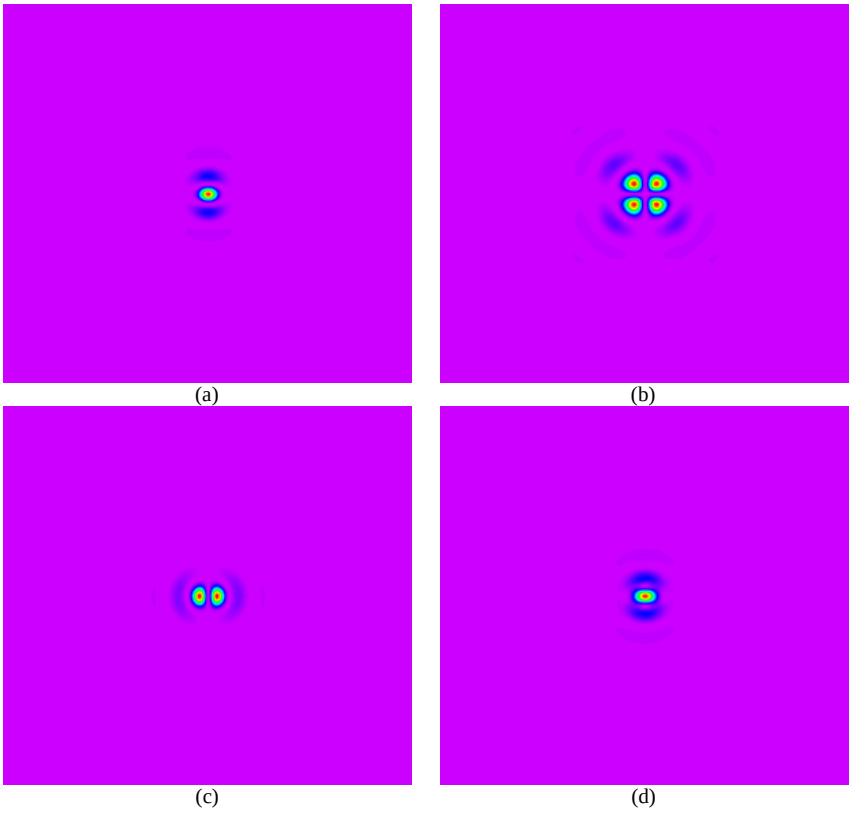

Fig. 3. The same as in Fig. 2 but now referred to the evanescent waves: (a) plot of $(|E_x|^2)_{ev}$; (b) $(|E_y|^2)_{ev}$; (c) $(|E_z|^2)_{ev}$; (d) $(|E_x|^2 + |E_y|^2 + |E_z|^2)_{ev}$. Integration throughout the transverse plane gives the values (a) 0.14; (b) 0.025; (c) 0.025; (d) 0.19.

#90265 - $15.00 USD Received 29 Nov 2007; revised 10 Jan 2008; accepted 24 Jan 2008; published 15 Feb 2008

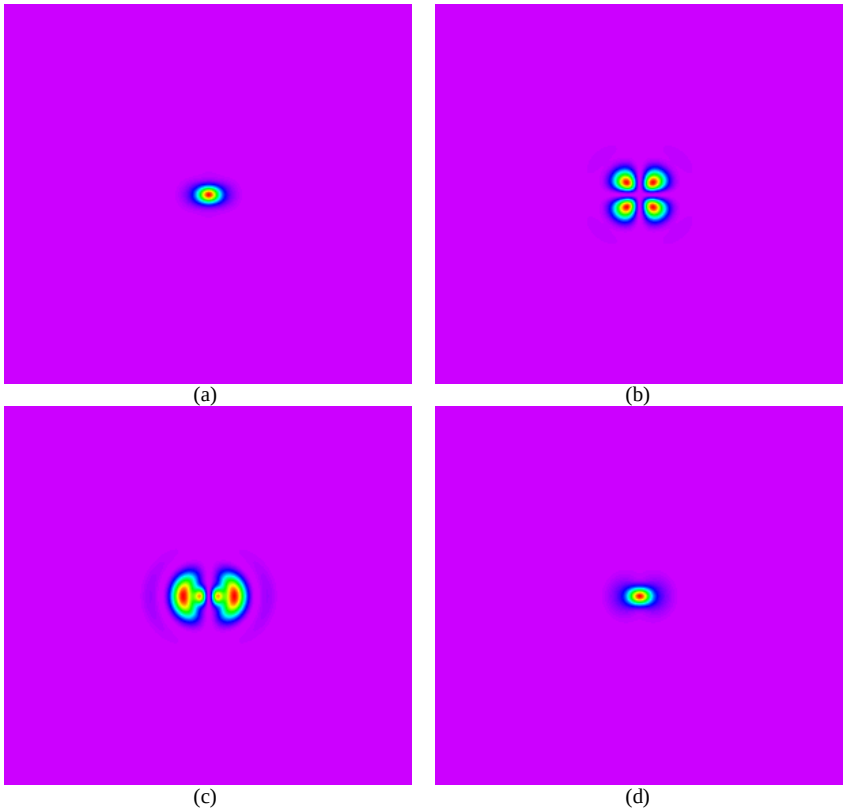

Fig. 4. The same as in Fig. 2 but now referred to the combined field (propagating + evanescent waves): (a) plot of $(|E_x|^2)_{pr+ev}$; (b) $(|E_y|^2)_{pr+ev}$; (c) $(|E_z|^2)_{pr+ev}$; (d) $(|E_x|^2 + |E_y|^2 + |E_z|^2)_{pr+ev}$. Integration throughout the transverse plane gives the values (a) 0.83; (b) 0.06; (c) 0.11; (d) 1.

#90265 - $15.00 USD Received 29 Nov 2007; revised 10 Jan 2008; accepted 24 Jan 2008; published 15 Feb 2008

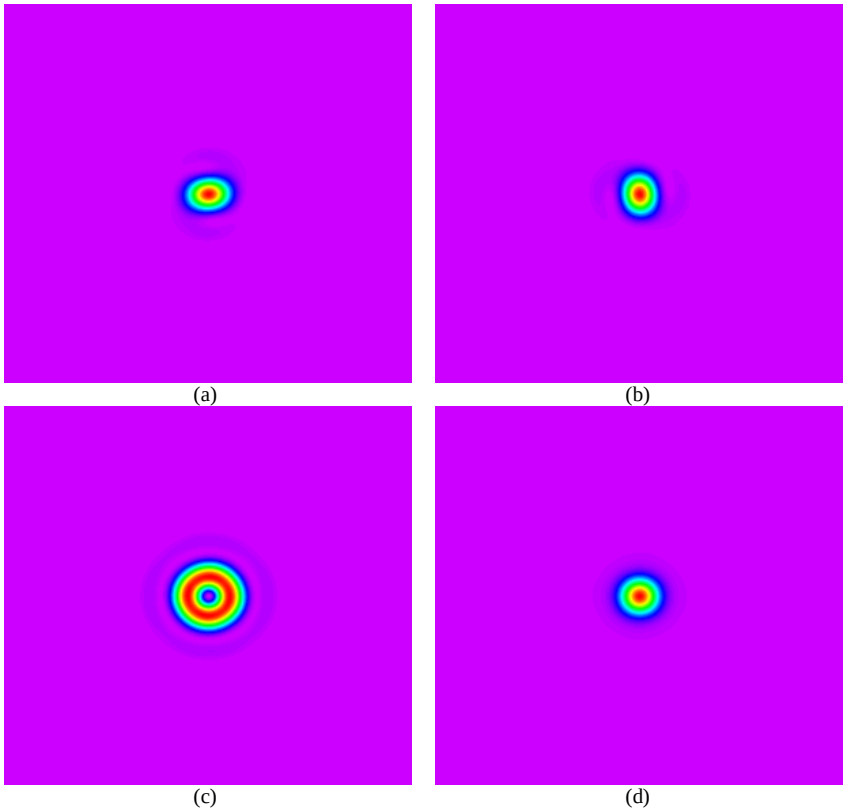

Fig. 5. The same as in Fig. 2 but now for the closest field associated to a circularly polarized Gaussian beam (see Eq. (20)). Integration over the entire transverse plane has now been normalised with respect to the value of Fig. 7.d (see below). (a) plot of $(|E_x|^2)_{pr}$; (b) $(|E_y|^2)_{pr}$; (c) $(|E_z|^2)_{pr}$; (d) $(|E_x|^2 + |E_y|^2 + |E_z|^2)_{pr}$. Integration throughout the transverse plane gives the values (a) 0.362; (b) 0.362; (c) 0.085; (d) 0.81.

#90265 - $15.00 USD Received 29 Nov 2007; revised 10 Jan 2008; accepted 24 Jan 2008; published 15 Feb 2008

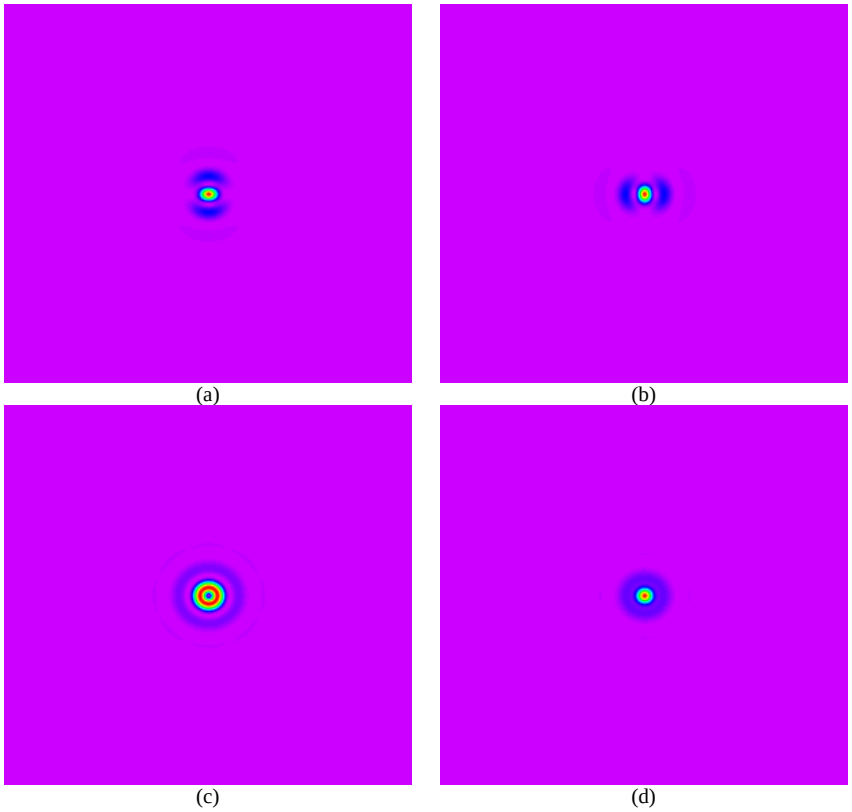

Fig. 6. The same as in Fig. 5 but now referred to the evanescent waves: (a) plot of $(|E_x|^2)_{ev}$; (b) $(|E_y|^2)_{ev}$; (c) $(|E_z|^2)_{ev}$; (d) $(|E_x|^2 + |E_y|^2 + |E_z|^2)_{ev}$. Integration throughout the transverse plane gives the values (a) 0.082; (b) 0.082; (c) 0.025; (d) 0.19.

#90265 - $15.00 USD Received 29 Nov 2007; revised 10 Jan 2008; accepted 24 Jan 2008; published 15 Feb 2008

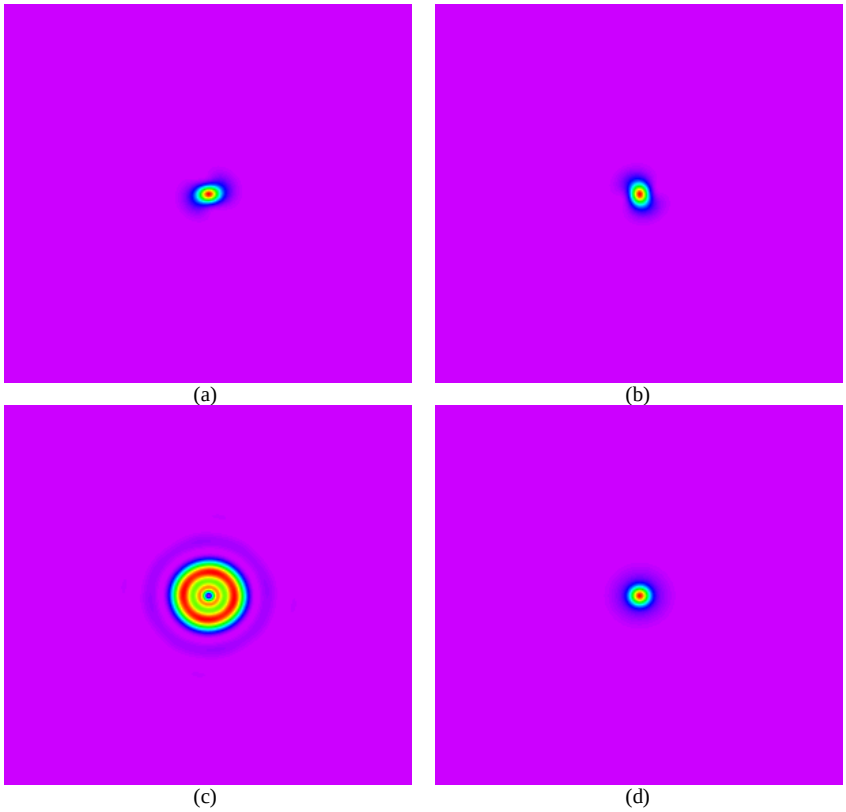

Fig. 7. The same as in Fig. 5 but now referred to the combined field (propagating + evanescent waves): (a) plot of $(|E_x|^2)_{pr+ev}$; (b) $(|E_y|^2)_{pr+ev}$; (c) $(|E_z|^2)_{pr+ev}$; (d) $(|E_x|^2 + |E_y|^2 + |E_z|^2)_{pr+ev}$. Integration throughout the transverse plane gives the values (a) 0.445; (b) 0.445; (c) 0.11; (d) 1.

5. Conclusions

Based on a certain choice of a reference vectorial system, the evanescent field associated to a kind of exact solutions of the Maxwell equations has been obtained in a simple way in terms of the angular spectrum of the field. The analytical expressions allow to directly compute (without introducing any approximation) both, the field magnitude and the polarization features of the evanescent waves. Moreover, since the exact solution has been decomposed into propagating and evanescent terms, the ranges of both, the beam size and the propagation distances can be easily determined for which the evanescent field is significant. The above general expressions have been applied to study the structure and the behaviour of the evanescent waves associated to the so-called closest field associated to the polarized Gaussian model. No confusion should arise between the evanescent field, obtained from Eq. (12) and (18), and the evanescent wave discussed in Ref. 26 for a polarized Gaussian beam. In that work, the angular spectrum representation was also considered, but a different treatment was used. Finally, the characteristics observed in the numerical examples have revealed to strongly depend on the type of polarization (linear or circular) of the Gaussian model.

Acknowledgements

Two authors (RMH and PMM) wish to thank the support of Ministerio de Educación y Ciencia (MEC) (project FIS2007-63396) and of CM-UCM (Research group 910335). The other author (AC) appreciates the support of MEC (project NAN2004-09348-C04-03). We also thank Dr. S. Bosch his interest and valuable help.

#90265 - $15.00 USD Received 29 Nov 2007; revised 10 Jan 2008; accepted 24 Jan 2008; published 15 Feb 2008